Chemical Engineering Journal 442 (2022) 136091

Contents lists available at ScienceDirect

Chemical Engineering Journal

journal homepage: www.elsevier.com/locate/cej

Integrated chamber-free microbial fuel cell for wastewater purification and bioenergy generation

Peng Chen [a], Taotao Zhang [a], Yahui Chen [a], Haitao Ma [b], Yu Wang [b], Wei Liu [c], Yao Wang [c], Guangwu Zhou [d], Renwei Qing [a], Yun Zhao [a], Heng Xu [a], Likai Hao [e,f], Can Wang [b,*], Fei Xu [a,*]

[a] Key Laboratory of Bio-Resource and Eco-Environment of Ministry of Education, College of Life Sciences, Sichuan University, Chengdu 610065, Sichuan, PR China
[b] School of Life Science and Engineering, Southwest Jiaotong University, Chengdu 610031, Sichuan, PR China
[c] Institute of New Energy and Low-Carbon Technology, Sichuan University, Chengdu 610065, Sichuan, PR China
[d] School of Aeronautics and Astronautics, Sichuan University, Chengdu 610065, Sichuan, PR China
[e] State Key Laboratory of Environmental Geochemistry, Institute of Geochemistry, CAS, Guiyang 550081, PR China
[f] CAS Center for Excellence in Quaternary Science and Global Change, Xi'an 710061, PR China

ARTICLE INFO

Keywords:
iMFC
Chamber free
Plug and use
Waste-energy transformation
Pseudocapacitance effect

ABSTRACT

An integrated chamber-free microbial fuel cell (iMFC) was constructed, which can be directly used for wastewater purification and energy recovery. The iMFC demonstrated potential electricity generating ability, producing 123.02 mW m^{-2} (688.90 mW m^{-3}) with an open-circuit voltage of 0.75 V and current discharge of 294.32 mAh. Cyclic voltammetry analysis indicated that the electricity storage capacity contributed by pseudocapacitance effect enhanced power generation of iMFC. Electrochemical impedance analysis revealed a low internal resistance (60.20 Ω), mainly related to internal diffusion. In addition, iMFC had an excellent chemical oxygen demand (COD) removal capacity, removing 81.20% of wastewater COD in 48 h, with optimum coulombic efficiency of 23.07%. The high-throughput sequencing analysis (16S rRNA/16S rDNA) indicated that *Comamonas*, *Delftia*, and *Flavobacterium* were dominant on both anode and cathode with varying abundance. Additionally, *Pseudomonas* and *Clostridium_sensu_stricto_13* contributed as important exoelectrogens. With concise architecture, the iMFC could be easily integrated and used in existing wastewater treatment plants without further construction, making it feasible for industrial application.

1. Introduction

In the past several decades, much effort has been put into the field of microbial fuel cells (MFC) and making biological power generation a reality. MFCs can convert various types of substrates into electricity, including acetate [1], glucose [2], *etc*. In 2004, a single-chamber MFC reactor constructed by Liu *et al*. generated 26 mW m^{-2} of electrical power with an 80.0% chemical oxygen demand (COD) removal rate from domestic wastewater, which demonstrated its power recovery feasibility while purifying wastewater [3].

In a MFC, electrochemically active microorganisms (EAMs) located on the anode could catalyze the anaerobic oxidation of organic matter [4]. During this process, the electrons produced by the microorganisms are transferred to the anode through electron mediators [5], nanowires [6], or membranes [7]. Then the electrons pass through a circuit to the cathode where they combine with protons and electron acceptors [8]. With the presence of the MFC anode, the degradation of organic pollutants could be promoted, because the anode serves as a stable and long-term electron acceptor for the electrons generated by the EAMs [9]. Therefore, the organic degrading efficiency in MFC is considered surpass the anaerobic process theoretically [10]. And MFC provides a different approach to extracting energy directly from wastewater and possibly turning a wastewater treatment plant into a power plant [11].

However, the complex architecture of MFCs limits their large-scale applications [11]. There are two basic configurations of the MFC system, namely the dual-chamber and signal chamber. The dual-chamber MFC consists of two reaction chambers (anode and cathode chamber) joined by a proton exchange membrane (PEM) [12], which blocks the transfer of dissolved oxygen or electron shuttles (such as ferricyanide, anthraquinone-2,6-disulfonate, *etc*.) to the anolyte, but allows the EAM-generated protons to diffuse into the catholyte [13]. However, due to high internal resistance caused by presence of the PEM, the power

* Corresponding authors at: No. 24 South Section 1, Yihuan Road, Chengdu 610065, PR China.
E-mail addresses: wangcan@swjtu.edu.cn (C. Wang), xufei@scu.edu.cn (F. Xu).

https://doi.org/10.1016/j.cej.2022.136091
Received 14 December 2021; Received in revised form 3 March 2022; Accepted 26 March 2022
Available online 30 March 2022

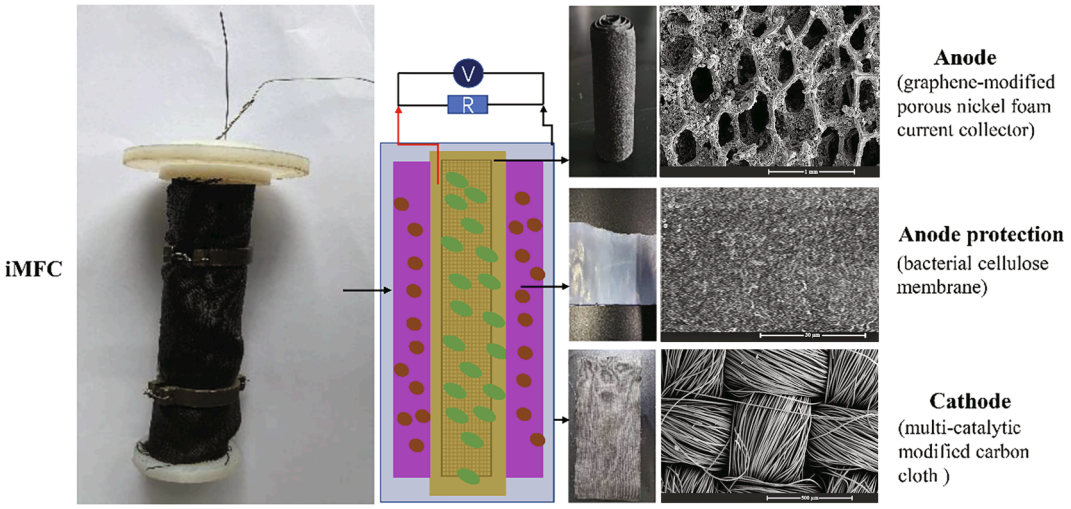

Fig. 1. The detailed configuration of iMFC. From left to right are individual iMFC photos, iMFC electrode configuration schematics, photos and scanned electron microscope characterization pictures of the main components of iMFC.

output by a two-chamber MFC is limited [12]. Moreover, additional catholyte is required due to the different nature of the electrodes. The single-chamber MFC directly exposes the cathode to air, and has a simpler configuration and better mass transfer performance [4].

Based on those designs, a variety of MFC configurations have been developed and investigated, such as the flat panel [14], stackable baffled [15], tubular [16], *etc*. Nevertheless, these MFCs still require the construction of reactors, which limit their practical application. As far as we know, only limited research focuses on the practical application scenario, and none of the MFCs are larger than one cubic meter, thus leading to a debate on whether MFC-based treatment plants can ever substitute the conventional wastewater treatment systems [11,17]. For example, Rodrigo *et al.* developed a membrane-less MFC, which has a high power output while treating wastewater, but maintenance of ancillary equipment is expensive [18]. The upflow membrane-less MFC designed by Mansoorian *et al.* has a large working volume, while the energy conversion efficiency is relatively low [19]. Zhang *et al.* developed a two-chamber MFC with high power density and coulombic efficiency, but its output performance decays rapidly after a period of operation [20]. To build MFC-based treatment plants or incorporate MFC (single or dual chamber) with the existing wastewater treatment plants, huge investment for new infrastructure constructions is needed, which makes the current MFC only feasible in the lab.

One possible solution is to simplify the configuration and directly integrate MFCs with current systems. To this end, we designed a prototype of the Integrated Chamber-free Microbial Fuel Cell (iMFC) assembly and tested it using artificial wastewater. Compared with the existing MFCs, the iMFC can be directly plugged in various environmental sites for power generation and wastewater purification, which presented stable organic-energy transformation in a long-term application, which does not require construction or reconstruction of the existing plants. With the incorporation of iMFC, the treatment efficiency of the existing wastewater treatment could be improved and the generated power could be used to power the plant operation. In this study, we report our preliminary findings on the electrochemical features of the prototype, electricity generation capability, and wastewater treatment capacity (removal of COD and total nitrogen). With its unique matrix clustering potential, iMFC is expected to be integrated into existing wastewater treatment plants to directly treat wastewater, thereby expanding the practical application areas of MFC.

2. Material and methods

2.1. Construction and operation

The anode was fabricated using a nickel foam, with graphene oxide deposited on the surface [21,22]. The nickel foam was then rolled into a column (diameter 20.0 mm, height 70.0 mm) for subsequent use. The cathode consisted of a 0.30 mm thick carbon cloth layer (wos1009; CeTech Co., Ltd., Taichung, Taiwan, China), which was ultrasonically cleaned with a mixture of HNO_3, NaOH, acetone, and deionized (DI) water for 30 min to remove impurities. Afterwards, the carbon cloth was cut and coated with a high-efficiency oxygen reduction catalyst combined with platinum and iron/nitrogen/carbon for subsequent use [23].

Before assembly, the anode was cultured anaerobically in a serum bottle for seven days, which was inoculated with anaerobic sludge from a local municipal wastewater treatment plant (Chengdu No.6 Sewage Treatment Plant, Sichuan, China). The stimulated wastewater contained 1.36 g L^{-1} $NaCH_3COO{\cdot}3H_2O$, 0.74 g L^{-1} KCl, 0.58 g L^{-1} NaCl, 0.68 g L^{-1} KH_2PO_4, 0.87 g L^{-1} K_2HPO_4, 0.28 g L^{-1} NH_4Cl, 0.1 g L^{-1} $MgSO_4{\cdot}7H_2O$, 0.1 g L^{-1} $CaCl_2{\cdot}2H_2O$, and 0.1 mL L^{-1} of a trace element mixture [24]. The trace mineral solution was consist of 2.0 g L^{-1} $FeCl_2{\cdot}4H_2O$, 0.05 g L^{-1} H_3BO_3, 0.05 g L^{-1} $ZnCl_2$, 0.03 g L^{-1} $CuCl_2$, 0.5 g L^{-1} $MnCl_2{\cdot}4H_2O$, 0.05 g L^{-1} $(NH_4)_6Mo_7O_{24}{\cdot}4H_2O$, 0.05 g L^{-1} $AlCl_3$, 0.05 g L^{-1} $CoCl_2{\cdot}6H_2O$, 0.05 g L^{-1} $NiCl_2$ [25].

After loading the microorganism, the anode column was tightly wrapped with a layer of bacterial cellulose (BC, 0.5 mm thick) using 10.0% polyvinyl alcohol (PVA, 1799 type; Aladdin, Shanghai, China) as adhesive. The cathode was then wrapped tightly on the BC layer. After attaching titanium wire (0.50 mm diameter) using a silver conductive epoxy (529 types; Ausbond (China) Co., Ltd., Suzhou, China), the electrodes were air-dried at ambient temperature for 4 h, and then the iMFC was obtained (The detailed configuration of the iMFC was shown in Fig. 1). The electrode surface area of a single iMFC is 14 cm^2 and the working volume is 250 mL.

During operation, the iMFC was placed in a 500 mL glass beaker (250 mL stimulated wastewater) and connected by titanium wires to an external circuit with a 1,000 Ω resistance. To ensure the long-term stable operation of iMFC, except for start-up operation (short-term open circuit), cyclic voltammetry test (short-time open circuit) and electrochemical impedance spectroscopy (open circuit) and output power density test (change different external resistance from 22 to 10,000 Ω), the iMFC was connected to 1,000 Ω external resistance. A data acquisition system with an integrated multichannel data acquisition device (DAQM4202 analog quantity acquisition module; Xi'an Zhouzheng

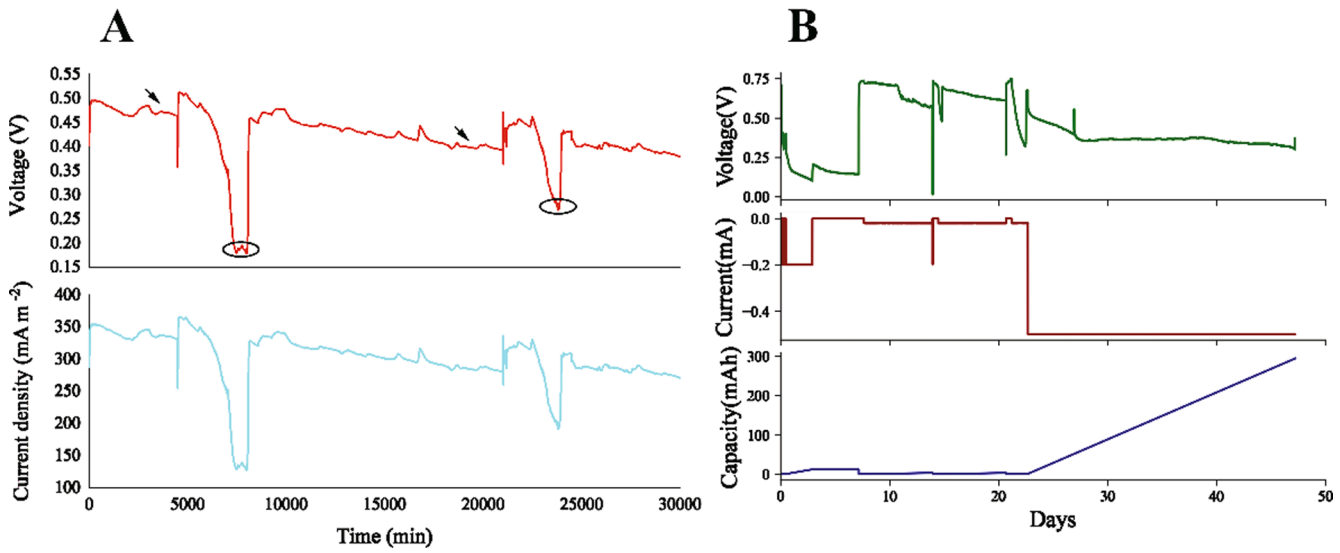

Fig. 2. iMFC electrical performance and power generation capacity curve. (A) The voltage–time graph (red curve) and current density-time graph (blue curve) of the initial stage of iMFC operation. (B) iMFC constant current discharge vs. time curve. The vertical axis from top to bottom is voltage (green curve), current (red curve) and capacity (blue curve). Notes: the black arrow indicated the change of stimulated wastewater.

Electronic Technology Co., Ltd., Xi'an, China) and an automatic data recording module (FT232 master photoelectric isolation surge protection USB to rs485; Future Technology Devices International Limited, Glasgow, UK) was connected in parallel at the ends of the resistance circuit to detect the working circuit voltage (WCV). The open-circuit voltage (OCV) was obtained by directly connecting the data acquisition system at the ends of the electrode set.

The iMFCs were operated in fed-batch mode replacing the medium at regular intervals (7 days). All the experiments were conducted at an ambient temperature of 15–25 °C. The details including the preparation procedure and composition of the stimulated wastewater can be found in Section 1 of the Supplementary information file.

2.2. Electrical performance analysis of the iMFC

Voltage stability and power generation capacity test. Besides monitoring with the multichannel data acquisition device, to determine the power generation capacity of the iMFC, a constant-current discharge test was performed at various current intensities (0.02, 0.20, 0.50 mA) using a land battery test system (CT2001A; Wuhan Land Electronics Co., Ltd., Wuhan, China) [26]. The generated electricity was stored as mAh, which indicated the capacity of the iMFC. The voltage of the iMFC during power generation was also recorded to evaluate its stability.

Cyclic Voltammetry (CV) analysis. To analyze the oxidation and reduction reaction process on electrodes, a CHI660E electrochemical workstation (Shanghai Chenhua Instrument Co., Ltd., Shanghai, China) was used to perform a CV test on the iMFC, using a 3.0 M Ag/AgCl saturated electrode (Shanghai Yue Magnetic Electronics Co., Ltd., Shanghai, China) [27]. Before the analysis, the iMFC was operated in an open circuit for 12 h until the system voltage was stabilized, and different scanning rate (1, 10, 20, 50, 100, and 200 mV s^{-1}) were used ranging from −1.0 to 1.0 V (Compared to the Ag/AgCl reference electrode). The pseudocapacitance and its contribution to the iMFC capacity were also calculated as described in the Supplementary materials Section 2 [28,29].

Electrochemical impedance spectroscopy (EIS). The EIS analysis was conducted to determine the internal resistance and study electrode dynamics. With tested the anode as the working electrode, the cathode as the counter electrode, and the Ag/AgCl electrode as the reference electrode. Subsequently, the working electrode of the electrochemical workstation was alternately connected to the iMFC anode and cathode. The impedance spectra were recorded by applying a sine wave (5 mV). The frequency range of the input AC signal during the test was 1 Hz ~ 1 M Hz [30,31]. The ZView-impedance Software (ZView 2.lnk) was used to fit the EIS data and plot the fitted curves. The ohmic resistance (R_s), constant phase element (CPE), charger transfer resistance (R_{ct}), and Warburg impedance (W_o) in the equivalent circuit were introduced in order to explain the electrode dynamics of the MFC (Fig. 4) [32].

2.3. Wastewater purification performance

The COD and total nitrogen (TN) were determined according to the Heuristic Algorithm for Clustering Hierarchy (HACH) protocol.

The COD removal efficiency and Coulombic efficiency (CE%) were calculated using the following equations [33]:

$$COD\ removal\ efficiency = \frac{COD_i - COD_t}{COD_i} \times 100\% \quad (1)$$

$$CE\% = \frac{8 \int I\ dt}{F \times V_{an} \times \Delta COD} \quad (2)$$

Where COD_i is the initial COD (mg L^{-1}); COD_t is the COD of the anolyte after iMFC operation; I is the current (A); F is the Faraday constant (96,485C mol^{-1}); V_{an} is the anode volume (mL); ΔCOD is the difference between the COD_i and COD_t (mg L^{-1}). The constant 8 was calculated and fixed based on the molecular weight of oxygen (32 g mol^{-1}) and assuming that 4 electrons are exchanged per mole of oxygen [16].

2.4. Characterization of the iMFC component materials

To determine the physical and morphological characteristics and the bacteria attachment, the electrode surface was monitored before and after the experimental run by field emission scanning electron microscopy (FE-SEM) using a JEOL Field Emission Scanning Electron Microscope (JEOL Ltd., Tokyo, Japan). The element distribution on the electrode was examined by energy-dispersive X-ray microanalysis (EDXMA) using a Kratos AXIS Ultra DLD X-ray Photoelectron Spectrometer (Kratos Analytical Ltd., Manchester, UK).

2.5. Microbial community analysis of the iMFC

To determine the evolution of the microbial community during iMFC

Table 1
Performance comparison of varied configured MFCs.

Reactor configuration	Chamber volume (L)	Power density (mW m^{-2}, Normalized by anode area)	CE (%, based on COD)	Constant current discharge capacity (mAh)	Practicability	Reference
Two-chamber MFC	1.00	25.00	Not mentioned	Not mentioned	New or retrofitted wastewater treatment facilities are required	18
Upflow membrane-less MFC	2.36	44.60	Not mentioned	Not mentioned	Idem	19
Two-chamber MFC	1.50	230.30	15.00	Not mentioned	Idem	20
Single-chamber circle MFC	1.89	Not mentioned	5.20	Not mentioned	Idem	45
Membrane-less	1.00	290.00	Not mentioned	Not mentioned	Idem	46
Twin-compartment MFC	1.80	93.00	Not mentioned	Not mentioned	Idem	47
iMFC	Chamber free	123.02	23.07	294.32	Plug and use	This study

operation, 16S rRNA and 16S rRNA gene high-throughput sequencing analysis was conducted. The bacterial DNA was extracted, and the bacterial RNA was extracted and inverse transcripted. After evaluating the quantity and quality of the extracted RNA and DNA using a NanoDrop NC2000 spectrophotometer (Thermo Fisher Scientific Inc., Waltham, MA, USA) and agarose gel electrophoresis, the V3-V4 hypervariable regions of the bacterial 16S rRNA gene were amplified with primers 338F (50-ACTCCTACGGGAGGCAGCAG-30) and 806R (50-GGACTACHVGGGTWTCTAAT-30). The amplicons were sequenced using the Illumina Novaseq platform (Illumina Inc., San Diego, CA, USA) at Shanghai Personal Biotechnology Co., Ltd. (Shanghai, China). Microbiome bioinformatics analysis was performed using QIIME2 2019.4 with slight modification according to the official user tutorials (https://docs.qiime2.org/2019.4/tutorials/)[34]. Sequence data analyses were mainly performed using QIIME2 and R packages (v3.2.0) to map the diversity of the iMFC microbial species at the genus level and calculate the Chao, Simpson, and Shannon indices, as well as the alpha diversity of the MFC bacterial community [35].

2.6. Statistical information

Mean and standard deviation values of three replicates were calculated by The R Programming Language (Version 4.1.1) [36]. All the tests were performed in triplicates (n = 3). The analysis of variance (ANOVA) was performed by R package plyr 1.8.6 [37] based on Fisher's least significant difference (LSD) procedure at a significance level of $P = 0.05$. All results were visualized by Data visualization package in R (Version 3.3.5) [38].

3. Results and discussion

3.1. The excellent generation capacity of the iMFC supports its large-scale applications

The voltage and current density change in the iMFC during operation revealed, as shown in Fig. 2, that the iMFC exhibited a high voltage, which always immediately increased to a maximum after the infusion of

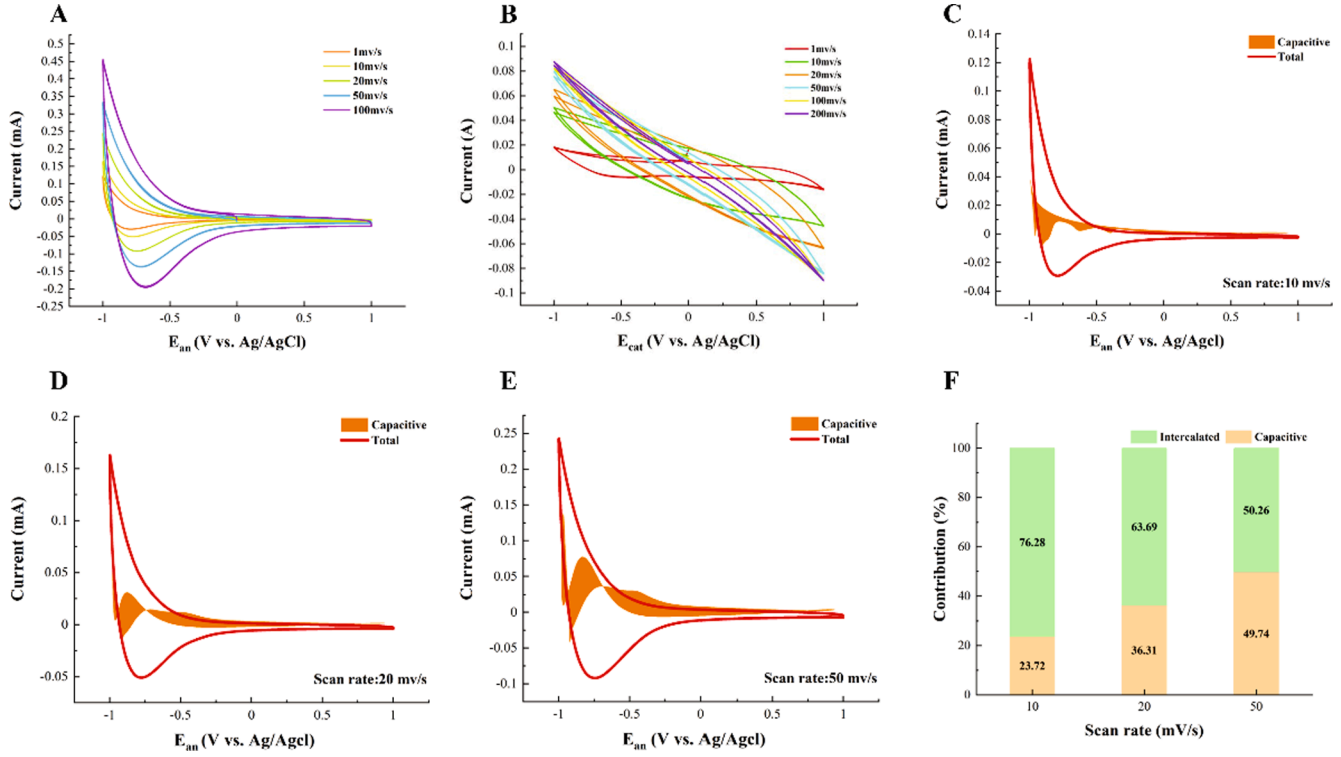

Fig. 3. iMFC cyclic voltammetry curve. (A) Anode CV curves at different scanning rates. (B) Cathode CV curves at different scanning rates. (C)-(E) The contribution of the pseudocapacitance effect in the MFC anode to the total capacity at different scanning rates (orange shaded area). (F) A stacked bar chart of the contribution of iMFC anode capacitor effect and diffusion control effect to total electric quantity at different scanning rates.

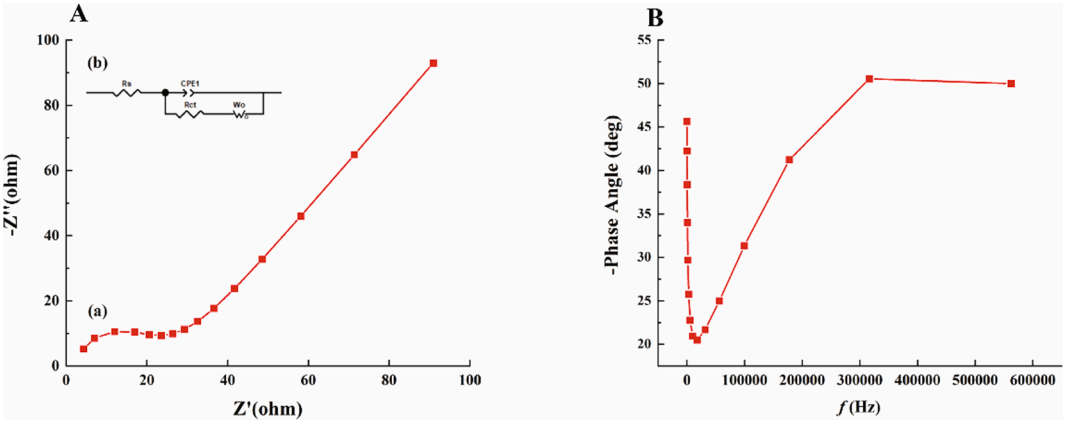

Fig. 4. Electrochemical impedance spectroscopy of iMFC. A a: Fitted Nyquist plot based on iMFC with frequency from 1 Hz to 1000 kHz. A b: Equivalent electrical circuits used to fit the EIS data. B: Phase-frequency Bode plot based on iMFC.

fresh wastewater. Under an external load of 1,000 Ω, the WCV maintained stable for 5000 mins with a maximum voltage of 0.51 V and a current density of 365.86 mA m^{-2}. With the change of wastewater, the WCV immediately elevated (the vertical curve with a black circle in Fig. 2A). However, the WCV decreased gradually from 0.51 to 0.18 V in about 360 min, then rapidly recovered to ~ 0.46 V and held steady (0.40–0.50 V) for a long time (1,5000 mins), until the "fuel" was exhausted and replaced. This unique "V-shaped" curve was different from the previous study and could be due to the unique configuration of iMFC. In the previous study about MFC, the WCV elevated with the refreshment of the substrate, but maintained and then gradually decreased with the exhaustion of the nutrient[39]. And no such decreased and bounced back phenomenon was observed[40].A possible explanation is that the EAMs inside the anode foam exhausted the nutrient absorbed by the reticular structure, but was shocked by the fresh wastewater, and the electron mediator generated by the EAMs was diluted by the fresh substrate, eventually causing the decline of the voltage. After a short time of adaptation, the EAM metabolism generated enough electron shuttle to maintain a faster electron transmission, leading to the bounced back of electricity [40,41].

Fig. 2B depicted the result of 48 days of long-term constant current discharge test. Before the test, the iMFC was in an open-circuit state with an OCV of 0.75 V. Different current discharge modes were used (0.02, 0.20, and 0.50 mA) for iMFC adaptation. Initially, the current was set to 0.20 mA, the medium intensity. The voltage of the iMFC dropped drastically, but the downward trend slowed down after a period of adaptation (on ~ 5th day). To prevent the collapse of the anode bacterial community, the discharge is temporarily terminated, and the voltage rapidly increases and then returned to the initial OCV. Subsequently, a low-intensity current (0.02 mA) was applied and the MFC voltage remained stable (between 0.50 and 0.75 V). After the voltage was stabilized, a high-intensity discharge (0.50 mA) was applied. Although the voltage initially decreased, it rapidly increased and then remained stable around 0.28–0.33 V for a long time. During the test, the iMFC capacity increased linearly after the high-intensity discharge (the capacity was 294.32 mAh on the 48th day).

The stable state of MFC is crutial for its practical application, which directly determines power output [42]. Many factors, including qualitative and quantitative changes in the anode biofilm, mass transfer obstruction by the dead microorganisms, the aging and community structure variation of EAMs, contamination of cathode catalyst, and change/exhaustion of substrate, *etc.*, will affect the long-term stability and performance of the MFC [39,43]. Especially, the excessive bacterial colonization would inhibit substrate diffusion and charge transfer. The irreversible damage of the anode biofilm due to the environmental changes (*e.g.*, strong water shock pressure) may result in a serious performance decline [44].

However, fortunately, due to the unique configuration (single-chamber, no membrane, rod electrode, cathode double-sided catalytic layer) and the high environmental adaptability of the microbiota, the iMFC maintained good stability during long-term operation (Fig. 2B), which guaranteed the long-term practical operation. Compared with other previously reported MFCs [18-20,45-47], iMFC of this study displayed a remarkable power generation capacity (Table 1). In particular, along with the firstly reported "plug and use" model, a constant electricity output was achieved in this study, making the iMFC highly attractive for future applications in practical energy recovery.

3.2. Remarkable energy storage capacity of the iMFC

As shown in Fig. 3, the anode CV curve had a typical asymmetrical shape, with a prominent reduction peak at a negative potential (from −1.0 V to −0.50 V). With the increase of the scanning rate, the position of the anode reduction peak shifted to the right, and the peak current and the integral area gradually increased (Fig. 3A). However, the cathode CV curve was relatively smooth with symmetrical positive and negative potentials and had no pronounced redox peak (Fig. 3B). It can be seen that the anodic electrochemical analysis of iMFC is more meaningful than the cathode. The CV curve can be used to indirectly determine the electron transfer mechanism occurringon the electrode. Two major electron transfer mechanisms occurred in the iMFC anode, namely the direct electron transfer process (DET) and indirect electron transfer process (IET) [48]. The DET process mainly occurs on the anode surface and the biofilm. The living cells of the biofilm consume the substrate (electron acceptor) and perform a series of enzymatic reactions. Then, electrons are generated and exported by the inherent electron-transfer mechanism, and part of the electrons is collected and transferred by the anode through the conductive structure (*e.g.*, nanowire) and extracellular enzymes (*e.g.*, cytochromes). The DET process only occurs when the conductive active site is close enough to the electrode surface. Some microorganisms (such as *Geobacter sulfurreducens*) contain conductive pili, which can extend tens of microns and be used as long-distance direct electron transfer cables (nanowires) [49,50]. The IET process is completed by electron mediators or shuttles (such as phenazine, H_2, or HS^-), which can carry electrons and react on the electrode surface [5,51].

Moreover, the rate-limiting current (around 0.025 mA, Fig. 3A) on the anode reached −0.37 V, indicating that a continuous, steady-state current connection was established between the anode biofilm and the electrode [48]. At the same time, as the voltage scanning rate increased, the rate-limiting current also gradually increased, indicating that the steady-state current generated between the electrode and the biofilm is greater at high scanning rate.

To further elucidate the kinetic mechanism of the electrode reaction,

pseudocapacitance analysis was performed on the anode at 10, 20, and 50 mV s^{-1} (Fig. 3C-E). Pseudocapacitance is not only generated on the surface of the electrode, but also within the entire electrode, so that a higher capacitance and energy density can be obtained than an electric double-layer capacitor [28]. Cyclic voltammetric pseudocapacitance testing is a powerful method to evaluate the electrochemical dynamics of electrodes. By fitting the current values at different scanning speeds, the k_1 value is obtained, and then the contribution ratio of the capacitance effect to the total capacity of the iMFC can be estimated (Fig. 3F) [29].

The area where the capacitance effect occurs (orange shaded part) was mainly found on both sides of the reduction peak of the anode CV curve, which concentrated in the negative potential area. Additionally, the contribution of the pseudocapacitance effect increased with the scanning rate, which increased from 23.72% (10 mV s^{-1}) to 36.61% (20 mV s^{-1}) and 49.74% (50 mV s^{-1}) (Fig. 3F, see Tab. S1 for detailed values). The contribution of the electric double layer capacitance to the total capacitance decreases as the scanning rate increases (from 72.68% (10 mV s^{-1}) to 63.69% (20 mV $s^{-1)}$ and 50.26% (50 mV s^{-1}) (Fig. 3F, green in the stacked histogram). The charge storage process dominated by pseudocapacitance and the ion diffusion process dominated by electric double-layer capacitors constitute a contribution to the total capacitance. It is worth noting that with the increase of the scanning rate, there was a significant pseudocapacitance effect on the CV curve of the anode, the contribution rate of pseudocapacitance to the total capacitance in iMFC increases significantly, and the contribution accounts for nearly half of the contribution at a scanning rate of 50 mV s^{-1} (Fig. 3F), which may be favorable for the energy storage of the iMFC [52,53]. For iMFC, the EAMs can use reductase on the cell membrane and self-produced mediators to temporarily store charges [54-56]. Also, a large number of electrons accumulated on the biofilm surface to form a capacitance. Electric double layer capacitors give iMFCs better charge–discharge rates, while pseudocapacitance give iMFCs better energy storage potential.

3.3. Small internal resistance reduces the energy loss of the iMFC

After fitting, the EIS results are presented in Nyquist form (Fig. 4). The high-frequency area curve is a relatively complete semi-circular arc, while the low-frequency area curve is a straight line with a 45° slope (Fig. 4A a). From the equivalent circuit diagram (Fig. 4A b), the internal ohmic resistance (R_s) of the iMFC was calculated to be 3.98 Ω, the charge / mass transfer internal resistance (R_{ct}) was 7.79 Ω, and the Warburg internal resistance (W_o-R) was 48.44 Ω. Also, the total internal resistance (R_{in}) was determined to be 60.20 Ω (Tab. S2). Such a small internal resistance led to better ion conductivity and electrical performance. The internal polarization resistance (defined as R_{ct} + W_o-R) accounts for a large proportion of the R_{in} [57]. In addition, the Bode plot (Fig. 4B) revealed that the region where the phase angle changed the most was located in the low and medium frequencies (~0–100000 Hz), while the phase angle in the high-frequency region remained stable, which is consistent with the results of the Nyquist plot.

The Nyquist diagram revealed that the Faraday impedance structure of the iMFC was complicated. In the high-frequency part, the capacitive reactance arc of the electric double layer dominated. However, in the low-frequency part, the diffusion control exceeded the electrochemical control, and Warburg impedance appears (the Nyquist diagram shows a 45° slope) [32].

The equivalent circuit is mainly based on the physical and chemical model of the contact between the electrode and the electrolyte. The resistor R_s represented the internal ohmic impedance, and indicated the resistance of the electrolyte and the anode surface, the cathode surface, and the H^+ produced by the anode, and then transported to the cathode [57]. The R_{ct} denotes the charge transfer resistance of the anode and cathode, which were inversely proportional to the chemical reaction rate of the electrodes. The constant component CPE1 corresponds to the

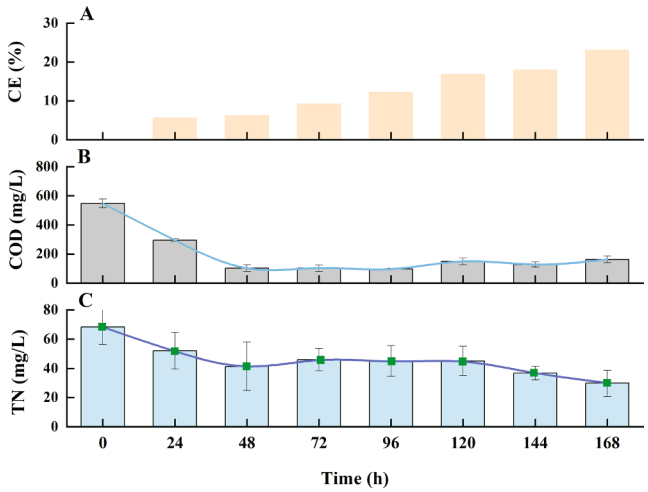

Fig. 5. Histogram of iMFC water treatment and coulombic efficiency for 168 h of continuous operation. (A) Coulombic efficiency. (B) Changes in the concentration of chemical oxygen demand in the device. (C) Changes in the concentration of total nitrogen in the device. The average value and sample standard deviations in the table were calculated based on the AVERAGE formula and the STEDEV.S formula in Microsoft Excel 2020 ("n" represents the number of samples, n = 3).

pseudocapacitance of the electric double layer at the electrochemical interface of the cathode/catholyte and the anode/anolyte [58]. The Warburg internal resistance (W_o-R) is used to reflect the characteristics of mixing the kinetics and charge transfer control [57], which is mainly reflected in the internal resistance of the diffusion process. A large W_o-R indicated that the ion diffusion process inside the iMFC was the main contributor to the internal resistance.

Relevant studies have shown that for MFCs operating at a fixed external resistance, the mature biofilms exhibit low internal resistance for polarization and charge transfer [59]. Additionally, the large polarization internal resistance indicated that the performance of the exchange current density was limited [57]. Although the polarization internal resistance in the iMFC was small (~56.23 Ω), it was also the main component of the internal resistance (93.40%). Thus, how to reduce the polarization internal resistance without reducing the main output performance is a problem that should be considered when optimizing the iMFC.

3.4. The iMFC converts energy to produce electricity while purifying water

To investigate the performance of the iMFC in wastewater treatment, the COD and TN were monitored during the whole treatment experiment. Before treatment, the wastewater has an initial practical COD of 548 ± 29.0 mg L^{-1} and TN of 68.33 ± 12.01 mg L^{-1} (with theoretical CON and TN at 600.0 and 70.0 mg L^{-1}, respectively).

The CE% was calculated to confirm the electron recovery capacity of the iMFC. During the operation, the CE% gradually increased from 5.50 to 23.07% (Fig. 5A), indicating that most of the COD did not participate in power generation. In the first 48 h, with the COD removal at 81.20%, the CE% reached only 6.17%, which is consistent with the findings of Logan *et al.* indicating that the water quality treatment and electricity generation of iMFC could be mutually obstructive [33].

The electron generation and transfer determine the coulombic efficiency. In this study, CE% gradually increased over time, indicating the enhanced performance of the iMFC. The activity of the cathode microbial flora, the diffusion of dissolved oxygen in the anode, the fermentation and methanation of some other non-EAMs in the anode will also affect the CE%. After the iMFC had been running for a long time, the viability and quantity of EAMs were constantly increasing, so that more COD was converted into electric energy, and then increased the

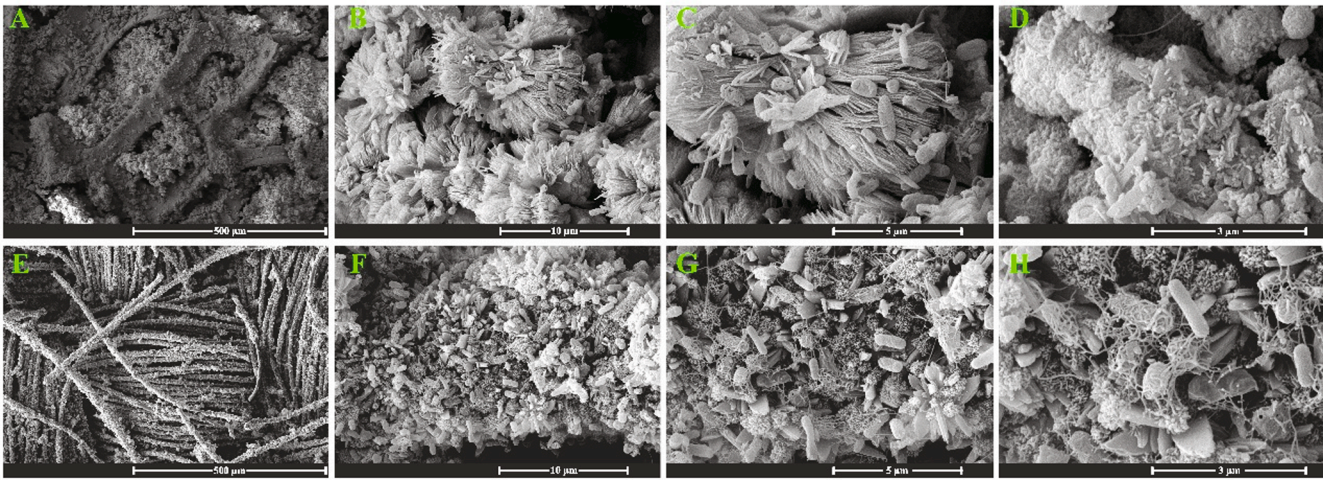

Fig. 6. Scanning electron microscope characterization of iMFC electrode material after long-term operation. (A-D) Characterization of anode materials under different magnifications. (E-H) Cathode material characterization under different magnifications.

electricity output. The above process eventually caused a well organic-energy transformation and a higher CE% than others (Table 1).

In 48 h, the iMFC removed 81.20% of the COD (Fig. 5B), with the COD decreasing from 548.00 to 103.00 mg L^{-1}. As the reaction continued, the COD showed no significant difference and ranged from 96.33 to 162.00 mg L^{-1} (Tab. S3), with the removal efficiency fluctuating between 70.44 and 82.42%. The iMFC can effectively maximize wastewater purification while generating electricity. In the closed circuit, the microbial flora on the anode provides electrons for the cathode reaction through the reduction degradation of organics, which can improve the biodegradation and electrochemical performance of the anode over time as the adaptation and evolution of the anode microbial flora occur [60]. The metabolism of the cathode microorganisms also contributes to the organic elimination in wastewater, mainly through aerobic degradation and the cathode can be considered as a deformed membrane bioreactor. In conclusion, the activity of EAMs and non-EAMs (in both electrodes) lead to the quick elimination of the COD [61].

In the first 48 h, the iMFC decreased the TN from 68.33 mg L^{-1} to 41.33 mg L^{-1}, resulting in 39.51% TN removal. At the end (168 h) of the experiment, the TN was decreased to 29.71 mg L^{-1} with a removal efficiency at 56.59% (Fig. 5C and Tab. S3). In the iMFC, the TN was eliminated through the following pathways, (1) nitrification effect and assimilation by the cathode biofilm [62]; (2) use of nitrate as the electron acceptor in the cathode [63]; (3) some bacteria on the anode can also consume nitrogen through the nitrate dissimilatory reduction reaction, which degrades dead cellular organism to obtain a carbon source [64]. Due to its "plug and use" property, the iMFC can be used as a potential alternative for the improvement of sewage treatment plants, as well as other environmental applications.

3.5. *The distinctive microstructure of the iMFC*

The iMFC was fabricated using a nickel foam column inside as the anode, a layer of bacterial cellulose in the middle as isolation, and a layer of catalyst-modified carbon cloth as the cathode (Fig. S1). The nickel foam has a porous structure composed of multiple hexagons. The graphene sheet evenly covered the foam surface. The numerous carbon nanofibres on the graphene sheet provided a large surface area for EAM (Fig. S1A). The EDS results showed that the material was mainly composed of carbon and nickel along with trace amounts of oxygen, sulfur, chloride, and sodium. After loading the EAM, a larger amount of differently shaped bacteria was observed, including long *bacillus*, short *bacillus*, and *coccus*, *etc* (Fig. S1D).

The carbon cloth (thickness 0.30 mm) was interwoven with carbon fiber (diameter 10 μm) (Fig. S1B). Before using it, both sides of the cloth were loaded with a highly-efficient Oxidation-Reduction Reactions (ORR) catalyst, which consisted of fluorine, sulfur, iron, and platinum, as indicated by EDS analysis (Fig. S1D). The bacterial cellulose layer was used to isolate the anode and cathode so as to prevent short circuits. As revealed by the SEM images, the layer was composed of nanofibers (~50 nm), which efficiently prevented the contraction of the anode and cathode without obstructing the mass transfer, including nutrients, electrons, and hydrogen (Fig. S1C).

After operation (Fig. 6), a loose and porous thick biofilm with multilayer formed on the anode (Fig. 6A-C), mainly containing rod-shaped and spherical bacteria, and many pili were also observed. Also, some large bacilli on the anode biofilm were stretched longer (Fig. 6C). The surface of some bacteria is evenly wrapped by extracellular substances, which might contribute to electricity production (Fig. 6C-D). The cathode was also coated with a biofilm (Fig. 6E-F), various filamentous or reticulated extracellular products were visible (Fig. 6F). Like the anode, many bacteria on the cathode were tightly entangled with mesh filaments (Fig. 6G-H). Also, there were many crystals and particles, which could be the debris of the iMFC components after long-term microbial erosion.

The loose and porous anode biofilm configuration increased the electrode surface area, expanded the ion reaction channel, and enable the anode to load more EAMs and extracellular polymeric substances (EPSs), which contributed to the formation of biofilms [65]. High EAM and EPS contents are beneficial to the power generation and stability of biofilms, respectively. Moreover, the bacterial pili also positively contributed to the charge transfer, which greatly improved the power generation of the iMFC [49]. Notably, some *bacilli* on the anode biofilm were stretched longer (Fig. 6C). Other related studies have also reported a similar phenomenon, which could be due to abnormal cell division under toxic stress [58,66]. In the iMFC in this study, the release and precipitation of nickel ions in the anode mediated by the bio-corrosion and formation of sulfides likely contributed to this phenomenon (Fig. S1D).

The structure of the cathode biofilm was more compact and rougher, and the bacteria were cross-linked to form a network (Fig. 6). An anode with a porous structure is conducive to the internal colonization of microorganisms, but micropores with a diameter of less than 10 μm are easily blocked due to the accumulation of metabolites and cell debris, thus inhibiting the mass and electron transfer. The formation of a cathode biofilm will also affect the long-term performance of the iMFC by preventing proton transfer to the catalyst [41]. The pores in the cathode could be blocked, thereby decreasing oxygen diffusion, which

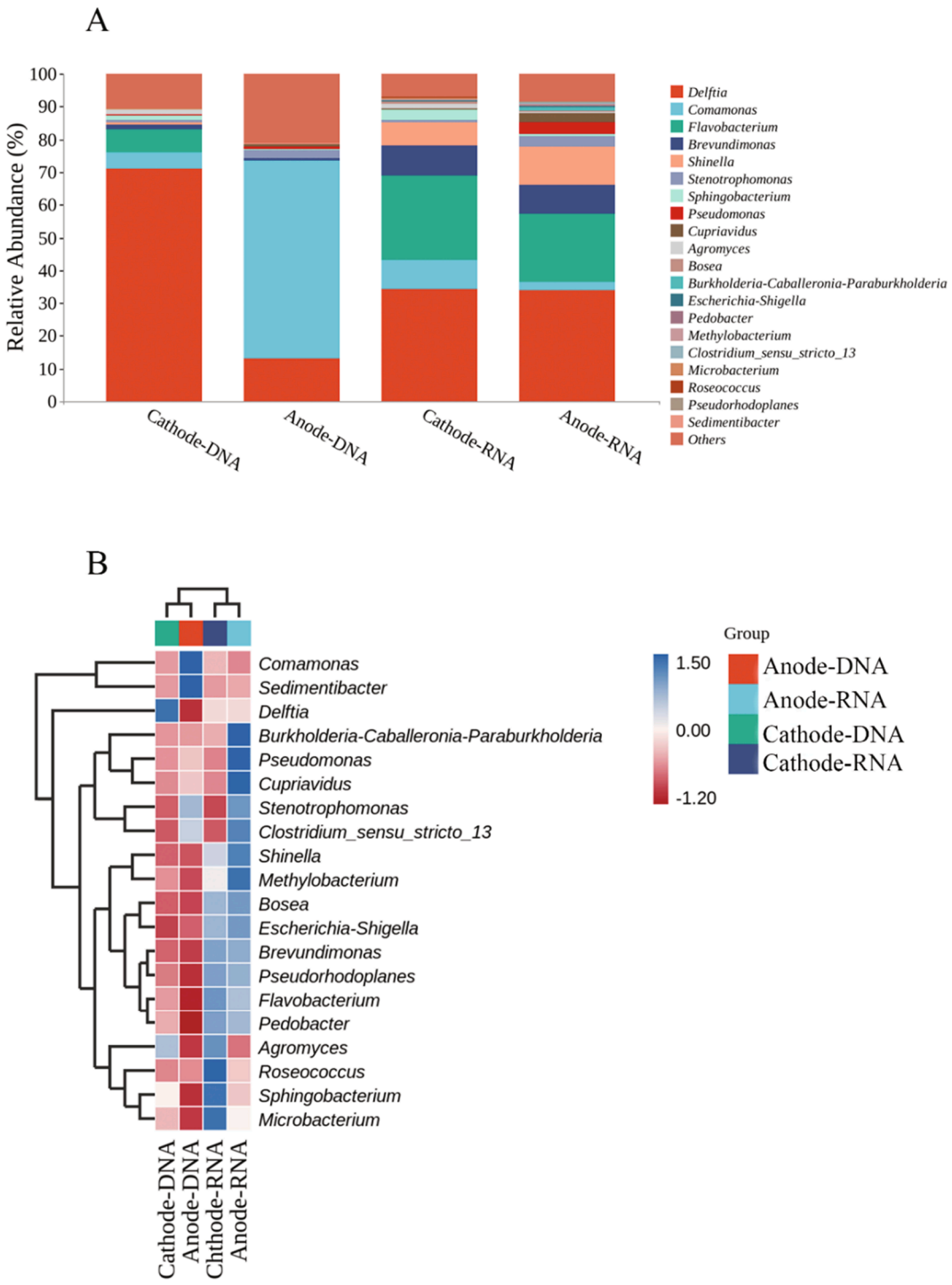

Fig. 7. A group diagram of 16S rDNA and 16S rRNA microbial community diversity analysis based on MFC anode and cathode. (A) Species taxonomic composition analysis of MFC anode and cathode microbial communities at the genus level (The figure shows the species with the top 20% abundance). (B) Species cluster analysis and species composition heatmap of MFC anode and cathode microbial communities at the genus level (The figure shows the species with the top 20% abundance. The sample clusters and species clusters are averaged and standardized by rows).

negatively affects the ORR reaction [42]. In addition, the precipitation of salts, including calcium, iron, nickel, magnesium (Fig. S1D), *etc*. will block the pore structure, reduce the exposure of electrochemically active sites, and inhibit reaction [67,68]. These factors should be taken into consideration when developing a long-term durable MFC for practical application, which guided our subsequent research on the iMFC.

3.6. Microbiome collaboration shapes the efficiency and stability of the iMFC

After operation, the microbial community of both electrodes of the iMFC was analyzed, and both 16S rDNA and 16S rRNA were sequenced to distinguish bacteria in different active states (Fig. 7). According to the analysis of the 16S rDNA sequencing data, the anode was mainly composed of *Comamonas* (60.45%), *Delftia* (13.09%), and others (21.10%), while the 16S rRNA sequencing data indicated that the anode

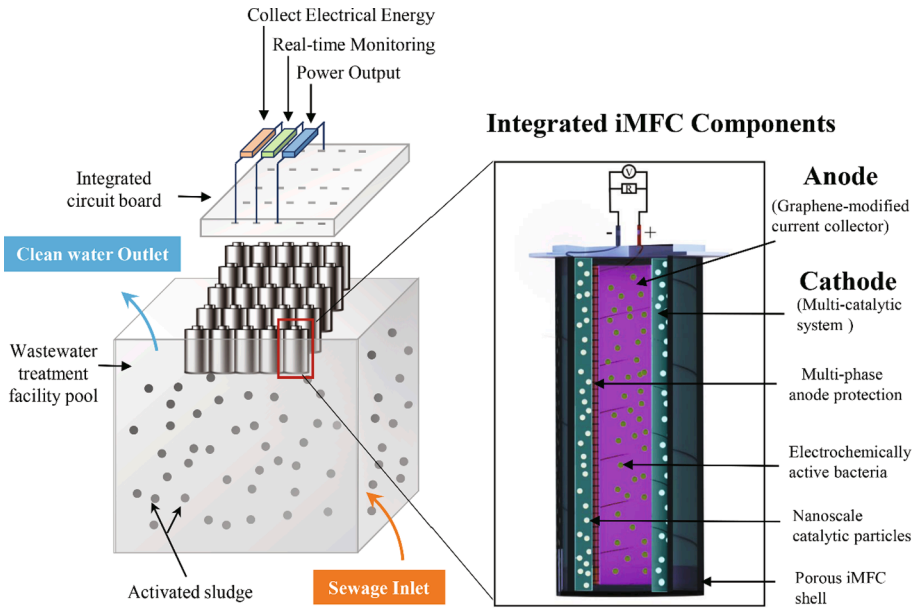

Fig. 8. iMFC actual wastewater treatment application schematic diagram.

was composed of *Delftia* (33.91%), *Flavobacterium* (20.80%), and *Shinella* (11.67%), *etc*. Unlike the anode, the cathode communities were mainly composed of *Delftia* (70.97% and 34.18%), *Flavobacterium* (7.16% and 25.65%), and *Comamonas* (4.88% and 9.04%), by 16S rDNA and 16S rRNA sequencing data, respectively (Tab. S4). Some bacteria related to electricity production, such as *Pseudomonas* and *Clostridium_sensu_stricto_13* were also present. The abundance of *Pseudomonas* in the anode according to 16S rDNA and 16S rRNA was 0.80% and 3.49%, respectively, which is much higher than that in the cathode (0.42% and 0.31%). *Clostridium_sensu_stricto_13* was only found in the anode (0.20% and 0.32% for 16S rDNA and 16S rRNA abundance, respectively).

The heatmap analysis revealed a huge difference in the microbial community in the anode and cathode according to both 16S rDNA and 16S rRNA sequencing data (Fig. 7B). For example, *Delftia* and *Agromyces* were the dominant genus on the anode, while their abundance on the cathode was low. At the same time, a significant proportion of the bacterial population was only detected by 16S rDNA sequencing, but not by 16S rRNA sequencing.

The Alpha diversity analysis performed on the iMFC microbiota Fig. S2) revealed a higher Chao1 index of bacterial comunnities on the anode, indicating a higher relative abundance of bacterial communities on the anode than on the cathode (Fig. S2A). The anode showed a higher Simpson and Shannon index value than the cathode (Fig. S2B-C), indicating that the community diversity of the anode bacteria was higher.

The microbial community is the most important component of an MFC. As microorganisms frequently found in natural and engineering environments, most *Comamonas* are heterotrophic organisms requiring oxidation [69-71], but some members (*e.g.*, *C. nitrativorans* and *C. denitrificans*) can use nitrate or ferric ion as electron acceptors[72]. *Comamonas* can catabolize a variety of substrates, including amino acids, carboxylic acids, steroids, and aromatic compounds [73-75], which have a great impact on the removal of organics from wastewater. *Delftia* (*Comamonas* family, β subclass of Proteobacteria) is widely found in river water, activated sludge, soil, and other environments [76]. It can tolerate high temperatures and degrade many kinds of organics at a high level, including DBP (dibutyl phthalate) [77] and aniline [78], and is also able to reduce nitrate to nitrite [79]. In this study, it was found that *Delftia* might play a crucial role in the elimination of nitrogen. *F. columnare*, another bacteria frequently found in sludge, usually grows in the form of biofilms and creates oxygen limiting conditions [80]. Its dominance in the anode contributed to the maintenance of an anaerobic environment and the function of EAMs, which probably also contributed to the good environment tolerant capacity of iMFC (capable of working under aerobic condition). *F. columnare* can perform denitrification by encoding enzymes that can reduce nitrate to nitrogen through the denitrification pathway [81], and grow anaerobically in the presence of nitrate [82], which has a positive effect on nitrogen removal.

Some flora in the iMFC directly contributed to the production of electricity, such as *Pseudomonas* and *Clostridium_sensu_stricto_13*. *Pseudomonas* is a common electrochemically active taxon, which is classified as a weak *exo*-electrogenic flora and a producer of low current density in the iMFC [83]. Certain species of *Pseudomonas*, *e.g.*, *Rhodopseudomonas palustris*, can generate higher power output after long-term acclimation [84]. Studies have shown that e-pili assembled from type IV fimbrin monomers can directly participate in the electronic energy transfer (EET) process [85], and can be formed by heterologous expression of the fimbrin gene of *Pseudomonas aeruginosa* [86]. *Clostridium_sensu_stricto_13* is only present on the anode, which was active (indicated by a higher RNA proportion than DNA). *Clostridium* has been demonstrated to have EET ability [87,88]. However, the current generation mechanism of *Clostridium* is relatively complex and remains unclear. More in-depth experiments and analysis are needed to understand the interaction between microorganisms in the MFC and the mechanism of electricity generation.

4. Conclusion and future perspective

The iMFC can be directly plugged for power generation and wastewater purification, which can stably operated in long-term application. The unique sleeve structure enable iMFC to tolerate and adapt to environmental changes, which does not require anaerobic condition. The low internal resistance and high pseudocapacitance effect contributed to its excellent performance, while the diffusion optimization could further improve the capacity. With the properties of small size, “plug and use”, durability, and tolerance capacity, iMFC could serve as a cleaner waste treatment and green energy source, contributing to global carbon neutralization. Hundreds of iMFCs can be assembled into an energy harvesting matrix (Fig. 8) directedly installed in sewage plants to power its operation (*e. g.* aeration). As the voltage cannot be increased by simply linking the iMFCs in series [89,90], the iMFCs should be wired to a power storage tank (such as a charge capacitor) and then discharge to

gain higher voltages. And a highly effective charge–discharge system is crucial for future application, especially when the current of the single cell is low (~mA).

Declaration of Competing Interest

The authors declare that they have no known competing financial interests or personal relationships that could have appeared to influence the work reported in this paper.

Acknowledgments

This study was financially supported by the Key Research and Development Program of Sichuan Province (2021YJ0495), the Fundamental Research Funds for the Central Universities (20826041D4303, 20826041E4314, 2682021CX084), the Startup Funding of the Chinese Academy of Sciences (2017-020), the Strategic Priority Research Program of Chinese Academy of Sciences (XDB40020300), the State Key Laboratory of Microbial Technology Foundation (M2017-01). The authors also wish to thank Professor Jian Zhao, Jie Zhang, Qun Sun from Sichuan University and Dr. Weizhen Fang from Analysis & Testing center, Southwest Jiaotong University.

Appendix A. Supplementary material

Supplementary data to this article can be found online at http://doi.org/10.1016/j.cej.2022.136091.

References

[1] A.E. Tugtas, P. Cavdar, B. Calli, Continuous flow membrane-less air cathode microbial fuel cell with spunbonded olefin diffusion layer, Bioresour. Technol. 102 (22) (2011) 10425–10430.
[2] N. Bourdakos, E. Marsili, R. Mahadevan, A defined co-culture of *Geobacter sulfurreducens* and *Escherichia coli* in a membrane-less microbial fuel cell, Biotechnol. Bioeng. 111 (4) (2014) 709–718.
[3] H. Liu, R. Ramnarayanan, B.E. Logan, Production of electricity during wastewater treatment using a single chamber microbial fuel cell, Environ. Sci. Technol. 38 (7) (2004) 2281–2285.
[4] H. Liu, S.A. Cheng, B.E. Logan, Production of electricity from acetate or butyrate using a single-chamber microbial fuel cell, Environ. Sci. Technol. 39 (2) (2005) 658–662.
[5] K. Rabaey, N. Boon, M. Höfte, W. Verstraete, Microbial phenazine production enhances electron transfer in biofuel cells, Environ. Sci. Technol. 39 (9) (2005) 3401–3408.
[6] Y.A. Gorby, S. Yanina, J.S. McLean, Electrically conductive bacterial nanowires produced by *Shewanella oneidensis* strain MR-1 and other microorganisms, PNAS 103 (30) (2006) 11358–11363.
[7] D.R. Bond, D.R. Lovley, Electricity production by *Geobacter sulfurreducens* attached to electrodes, Appl. Environ. Microbiol. 69 (3) (2003) 1548–1555.
[8] R. Rossi, X. Wang, B.E. Logan, High performance flow through microbial fuel cells with anion exchange membrane, J. Power Sources 475 (2020), 228633.
[9] D.R. Lovley, K.P. Nevin, A shift in the current: new applications and concepts for microbe-electrode electron exchange, Curr. Opin. Biotechnol. 22 (3) (2011) 441–448.
[10] D. Cheng, H.H. Ngo, W. Guo, Evaluation of a continuous flow microbial fuel cell for treating synthetic swine wastewater containing antibiotics, Sci. Total Environ. 756 (2021), 144133.
[11] B.E. Logan, M. Elimelech, Membrane-based processes for sustainable power generation using water, Nature 488 (7411) (2012) 313–319.
[12] B.E. Logan, B. Hamelers, R. Rozendal, Microbial fuel cells: methodology and technology, Environ. Sci. Technol. 40 (17) (2006) 5181–5192.
[13] B.E. Logan, Microbial Fuel Cells, John Wiley & Sons, New York, 2008.
[14] Y. Park, J. Yu, V.K. Nguyen, Understanding complete ammonium removal mechanism in single-chamber microbial fuel cells based on microbial ecology, Sci. Total Environ. 764 (2021), 144231.
[15] Y. Dong, Y. Qu, W. He, Y. Du, J. Liu, X. Han, Y. Feng, A 90-liter stackable baffled microbial fuel cell for brewery wastewater treatment based on energy self-sufficient mode, Bioresour. Technol. 195 (2015) 66–72.
[16] K. Rabaey, P. Clauwaert, P. Aelterman, W. Verstraete, Tubular microbial fuel cells for efficient electricity generation, Environ. Sci. Technol. 39 (20) (2005) 8077–8082.
[17] P.L. McCarty, J. Bae, J. Kim, Domestic wastewater treatment as a net energy producer—can this be achieved? Environ. Sci. Technol. 45 (17) (2011) 7100–7106.
[18] M.A. Rodrigo, P. Cañizares, J. Lobato, R. Paz, C. Sáez, J.J. Linares, Production of electricity from the treatment of urban waste water using a microbial fuel cell, J. Power Sources 169 (1) (2007) 198–204.
[19] H.J. Mansoorian, A.H. Mahvi, A.J. Jafari, M.M. Amin, A. Rajabizadeh, N. Khanjani, Bioelectricity generation using two chamber microbial fuel cell treating wastewater from food processing, Enzyme Microb. Technol. 52 (6-7) (2013) 352–357.
[20] Y. Zhang, L.G. Olias, P. Kongjan, I. Angelidaki, Submersible microbial fuel cell for electricity production from sewage sludge, Water Sci. Technol. 64 (1) (2011) 50–55.
[21] W. Liu, H. Li, J. Jin, Y. Wang, Z. Zhang, Z. Chen, Q. Wang, Y. Chen, E. Paek, D. Mitlin, Synergy of epoxy chemical tethers and defect-free graphene in enabling stable lithium cycling of silicon nanoparticles, Angew. Chem. Int. Ed. 58 (46) (2019) 16590–16600.
[22] P. Jiang, Y. Liao, W. Liu, Y. Chen, Alternating nanolayers as lithiophilic scaffolds for Li-metal anode, Journal of Energy, Chemistry 57 (2021) 131–139.
[23] Y. Liao, Y. Wang, R. Zhang, C. Wu, Y. Yan, Y. Chen, Anti-sintering Pt particles confined in short ordered mesoporous carbon with rapid mass transport for superior and robust oxygen reduction, ChemCatChem 12 (7) (2020) 1958–1962.
[24] P. Kuntke, K.M. Śmiech, H. Bruning, G. Zeeman, M. Saakes, T.H.J.A. Sleutels, H.V. M. Hamelers, C.J.N. Buisman, Ammonium recovery and energy production from urine by a microbial fuel cell, Water Res. 46 (8) (2012) 2627–2636.
[25] A.J.B. Zehnder, B.A. Huser, T.D. Brock, K. Wuhrmann, Characterization of an acetate-decarboxylating, non-hydrogen-oxidizing methane bacterium, Arch. Microbiol. 124 (1) (1980) 1–11.
[26] F. Liu, C.Y. Wang, Water and methanol crossover in direct methanol fuel cells—Effect of anode diffusion media, Electrochim. Acta 53 (24) (2008), 7357 7357.
[27] C.I. Torres, A.K. Marcus, P. Parameswaran, B.E. Rittmann, Kinetic experiments for evaluating the Nernst-Monod model for anode-respiring bacteria (ARB) in a biofilm anode, Environ. Sci. Technol. 42 (17) (2008) 6593–6597.
[28] F. Soavi, L.G. Bettini, P. Piseri, Miniaturized supercapacitors: key materials and structures towards autonomous and sustainable devices and systems, J. Power Sources 326 (2016) 717–725.
[29] C. Costentin, J.M. Savéant, Energy storage: pseudocapacitance in prospect, Chem. Sci. 10 (22) (2019) 5656–5666.
[30] Z. Wen, S. Ci, F. Zhang, X. Feng, S. Cui, S. Mao, S. Luo, Z. He, J. Chen, Nitrogen-enriched core-shell structured Fe/Fe_3C-C nanorods as advanced electrocatalysts for oxygen reduction reaction, Adv. Mater. 24 (11) (2012) 1399–1404.
[31] F. Zhang, M.D. Merrill, J.C. Tokash, T. Saito, S. Cheng, M.A. Hickner, B.E. Logan, Mesh optimization for microbial fuel cell cathodes constructed around stainless steel mesh current collectors, J. Power Sources 196 (3) (2011) 1097–1102.
[32] C.C. Chang, W. Kao, C.P. Yu, Assessment of voltage reversal effects in the serially connected biocathode-based microbial fuel cells through treatment performance, electrochemical and microbial community analysis, Chem. Eng. J. 397 (2020), 125368.
[33] S. Cheng, H. Liu, B.E. Logan, Power densities using different cathode catalysts (Pt and CoTMPP) and polymer binders (nafion and PTFE) in single chamber microbial fuel cells, Environ. Sci. Technol. 40 (1) (2006) 364–369.
[34] E. Bolyen, J.R. Rideout, M.R. Dillon, Reproducible, interactive, scalable and extensible microbiome data science using QIIME 2, Nat. Biotechnol. 37 (8) (2019) 852–857.
[35] C. Wang, H. Tan, H. Li, Mechanism study of Chromium influenced soil remediated by an uptake-detoxification system using hyperaccumulator, resistant microbe consortium, Environ. Pollut. 257 (2020), 113558.
[36] R. Team, R: A language and environment for statistical computing, The R Development Core Team (2021).
[37] H. Wickham, The split-apply-combine strategy for data analysis, J. Stat. Softw. 40 (1) (2011) 1–29.
[38] V. Gómez-Rubio, ggplot2—elegant graphics for data analysis (2nd Edition), Journal of Statistical Software 77(b02) (2017).
[39] A.A. Carmona-Martínez, E. Trably, K. Milferstedt, R. Lacroix, L. Etcheverry, N. Bernet, Long-term continuous production of H_2 in a microbial electrolysis cell (MEC) treating saline wastewater, Water Res. 81 (2015) 149–156.
[40] J. Wu, W. Zhang, K. Chai, Corrosion behavior of AISI 1045 steel in seawater in the presence of *Flavobacterium* sp, Front. Microbiol. 11 (2020) 303.
[41] D. Nath, I. Chakraborty, M.M. Ghangrekar, Methanogenesis inhibitors used in bio-electrochemical systems: A review revealing reality to decide future direction and applications, Bioresour. Technol. 319 (2021), 124141.
[42] J. Menicucci, H. Beyenal, E. Marsili, Procedure for determining maximum sustainable power generated by microbial fuel cells, Environ. Sci. Technol. 40 (3) (2006) 1062–1068.
[43] J. Hashemi, A. Samimi, Steady state electric power generation in up-flow microbial fuel cell using the estimated time span method for bacteria growth domestic wastewater, Biomass Bioenergy 45 (2012) 65–76.
[44] X. Xie, M. Ye, L. Hu, N. Liu, J.R. McDonough, W. Chen, H.N. Alshareef, C. S. Criddle, Y.i. Cui, Carbon nanotube-coated macroporous sponge for microbial fuel cell electrodes, Energy Environ. Sci. 5 (1) (2012) 5265–5270.
[45] J. Cheng, X. Zhu, J. Ni, A. Borthwick, Palm oil mill effluent treatment using a two-stage microbial fuel cells system integrated with immobilized biological aerated filters, Bioresour. Technol. 101 (8) (2010) 2729–2734.
[46] L. Damiano, J.R. Jambeck, D.B. Ringelberg, Municipal solid waste landfill leachate treatment and electricity production using microbial fuel cells, Appl. Biochem. Biotechnol. 173 (2) (2014) 472–485.
[47] Y. Lee, N. Nirmalakhandan, Electricity production in membrane-less microbial fuel cell fed with livestock organic solid waste, Bioresour. Technol. 102 (10) (2011) 5831–5835.

[48] C.W. Marshall, H.D. May, Electrochemical evidence of direct electrode reduction by a thermophilic Gram-positive bacterium, *Thermincola ferriacetica*, Energy & Environmental Science 2 (6) (2009) 699–705.
[49] G. Reguera, K.D. McCarthy, T. Mehta, J.S. Nicoll, M.T. Tuominen, D.R. Lovley, Extracellular electron transfer via microbial nanowires, Nature 435 (7045) (2005) 1098–1101.
[50] G. Reguera, K.P. Nevin, J.S. Nicoll, S.F. Covalla, T.L. Woodard, D.R. Lovley, Biofilm and nanowire production leads to increased current in *Geobacter sulfurreducens* fuel cells, Appl. Environ. Microbiol. 72 (11) (2006) 7345–7348.
[51] H. von Canstein, J. Ogawa, S. Shimizu, J.R. Lloyd, Secretion of flavins by *Shewanella* species and their role in extracellular electron transfer, Appl. Environ. Microbiol. 74 (3) (2008) 615–623.
[52] M. Forghani, S.W. Donne, Complications when differentiating charge transfer processes in electrochemical capacitor materials: assessment of cyclic voltammetry data, J. Electrochem. Soc. 166 (8) (2019) A1370–A1379.
[53] P. Simon, Y. Gogotsi, Materials for electrochemical capacitors, Nat. Mater. 7 (11) (2008) 845–854.
[54] A.T. Heijne, D. Liu, M. Sulonen, T. Sleutels, F. Fabregat-Santiago, Quantification of bio-anode capacitance in bioelectrochemical systems using Electrochemical Impedance Spectroscopy, J. Power Sources 400 (2018) 533–538.
[55] Z. Lv, D. Xie, F. Li, Y. Hu, C. Wei, C. Feng, Microbial fuel cell as a biocapacitor by using pseudo-capacitive anode materials, J. Power Sources 246 (2014) 642–649.
[56] X. Peng, H. Yu, H. Yu, X. Wang, Lack of anodic capacitance causes power overshoot in microbial fuel cells, Bioresour. Technol. 138 (2013) 353–358.
[57] X. Dominguez-Benetton, S. Sevda, K. Vanbroekhoven, D. Pant, The accurate use of impedance analysis for the study of microbial electrochemical systems, Chem. Soc. Rev. 41 (21) (2012) 7228.
[58] M.S. Bashir, Benign fabrication process of hierarchal porous polyurea microspheres with tunable pores and porosity: Their Pd immobilization and use for hexavalent chromium reduction, Chem. Eng. Res. Des. 175 (2021) 102–114.
[59] S. Srikanth, E. Marsili, M.C. Flickinger, D.R. Bond, Enrico, Electrochemical characterization of *Geobacter sulfurreducens* cells immobilized on graphite paper electrodes, Biotechnol. Bioeng. 99 (5) (2008) 1065–1073.
[60] Y. Wu, Q. Yang, Q. Zeng, H.H. Ngo, W. Guo, H. Zhang, Enhanced low C/N nitrogen removal in an innovative microbial fuel cell (MFC) with electroconductivity aerated membrane (EAM) as biocathode, Chem. Eng. J. 316 (2017) 315–322.
[61] X. Su, Y. Tian, Z. Sun, Y. Lu, Z. Li, Performance of a combined system of microbial fuel cell and membrane bioreactor: Wastewater treatment, sludge reduction, energy recovery and membrane fouling, Biosens. Bioelectron. 49 (22) (2013) 92–98.
[62] P. Clauwaert, K. Rabaey, P. Aelterman, L. De Schamphelaire, T.H. Pham, P. Boeckx, N. Boon, W. Verstraete, Biological denitrification in microbial fuel cells, Environ. Sci. Technol. 41 (9) (2007) 3354–3360.
[63] Y. Xiao, S. Wu, Z.-H. Yang, Z.-J. Wang, C.-Z. Yan, F. Zhao, In situ probing the effect of potentials on the microenvironment of heterotrophic denitrification biofilm with microelectrodes, Chemosphere 93 (7) (2013) 1295–1300.
[64] Y. Xiao, Y. Zheng, S. Wu, Z.-H. Yang, F. Zhao, Bacterial community structure of autotrophic denitrification biocathode by 454 pyrosequencing of the 16S rRNA gene, Microb. Ecol. 69 (3) (2015) 492–499.
[65] Z. Zhang, R. Cao, L. Jin, W. Zhu, Y. Ji, X. Xu, L. Zhu, The regulation of N-acyl-homoserine lactones (AHLs)-based quorum sensing on EPS secretion via ATP synthetic for the stability of aerobic granular sludge, The Science of the Total Environment 673 (2019) 83–91.
[66] F. Liu, M. Xu, X. Chen, A novel strategy for tracking the microbial degradation of azo dyes with different polarity in living cells, Environ. Sci. Technol. 49 (19) (2015) 11356–11362.
[67] C. Santoro, A. Stadlhofer, V. Hacker, G. Squadrito, U. Schröder, B. Li, Activated carbon nanofibers, J. Power Sources 243 (2013) 499–507.
[68] Z. Fang, D. Pant, B.E. Logan, Long-term performance of activated carbon air cathodes with different diffusion layer porosities in microbial fuel cells, Biosens. Bioelectron. 30 (1) (2011) 49–55.
[69] O. Auguet, M. Pijuan, H. Guasch-Balcells, C.M. Borrego, O. Gutierrez, Implications of Downstream Nitrate Dosage in anaerobic sewers to control sulfide and methane emissions, Water Res. 68 (2015) 522–532.
[70] A. Sotres, M. Cerrillo, M. Viñas, Nitrogen removal in a two-chambered microbial fuel cell: Establishment of a nitrifying-denitrifying microbial community on an intermittent aerated cathode, Chem. Eng. J. 284 (2016) 905–916.
[71] Y. Guo, H. Gong, X. Guo, Rhizosphere bacterial community of *Typha angustifolia* L. and water quality in a river wetland supplied with reclaimed water, Appl. Microbiol. Biotechnol. 99 (6) (2015) 2883–2893.
[72] C.Y. Wu, L. Zhuang, S.G. Zhou, Fe(III) inhanced anaerobic transformation of 2,4-dichlorophenoxyacetic acid by an iron-reducing bacterium *Comamonas koreensis* CY01, FEMS Microbiol. Ecol. 71 (1) (2010) 106–113.
[73] N. Boon, J. Goris, P. De Vos, W. Verstraete, E.M. Top, Bioaugmentation of Activated Sludge by an Indigenous 3-Chloroaniline-Degrading *Comamonas testosteroni* Strain, I2gfp, Appl. Environ. Microbiol. 66 (7) (2000) 2906–2913.
[74] L. Liu, C.-Y. Jiang, X.-Y. Liu, J.-F. Wu, J.-G. Han, S.-J. Liu, Plant-microbe association for rhizoremediation of chloronitroaromatic pollutants with *Comamonas* sp. strain CNB-1, Environ. Microbiol. 9 (2) (2007) 465–473.
[75] J.-F. Wu, C.-Y. Jiang, B.-J. Wang, Y.-F. Ma, Z.-P. Liu, S.-J. Liu, Novel partial reductive pathway for 4-chloronitrobenzene and nitrobenzene degradation in *Comamonas* sp. strain CNB-1, Appl. Environ. Microbiol. 72 (3) (2006) 1759–1765.
[76] T. Shigematsu, K. Yumihara, Y. Ueda, M. Numaguchi, S. Morimura, K. Kida, *Delftia tsuruhatensis* sp. nov., a terephthalate-assimilating bacterium isolated from activated sludge, Microbiology Society 53 (5) (2003) 1479–1483.
[77] N.K. Patil, R. Kundapur, Y.S. Shouche, Degradation of plasticizer di-n-butylphthalate by *Delftia* sp. TBKNP-05, Curr. Microbiol. 52 (3) (2006) 225–230.
[78] Z. Liu, H. Yang, Z. Huang, Degradation of aniline by newly isolated, extremely aniline-tolerant *Delftia* sp. AN3, Appl. Microbiol. Biotechnol. 58 (5) (2002) 679–682.
[79] M.A. Morel, M.C. Ubalde, V. Braña, *Delftia* sp. JD2: a potential Cr(VI)-reducing agent with plant growth-promoting activity, Arch. Microbiol. 193 (1) (2011) 63–68.
[80] W. Cai, L. De, La Fuente, C.R. Arias, Biofilm formation by the fish pathogen *Flavobacterium columnare*: Development and parameters affecting surface attachment, Appl. Environ. Microbiol. 79 (18) (2013) 5633–5642.
[81] H. Abdelhamed, S.W. Nho, A. Karsi, M.L. Lawrence, The role of denitrification genes in anaerobic growth and virulence of *Flavobacterium columnare*, J. Appl. Microbiol. 130 (4) (2021) 1062–1074.
[82] H.C. Tekedar, K. Attila, J.S. Reddy, Comparative genomics and transcriptional analysis of *Flavobacterium columnare* strain ATCC 49512, Front. Microbiol. 8 (2017) 588.
[83] L.E. Doyle, E. Marsili, Weak electricigens: A new avenue for bioelectrochemical research, Bioresour. Technol. 258 (2018) 354–364.
[84] H. Yi, K.P. Nevin, B.-C. Kim, A.E. Franks, A. Klimes, L.M. Tender, D.R. Lovley, Selection of a variant of *Geobacter sulfurreducens* with enhanced capacity for current production in microbial fuel cells, Biosens. Bioelectron. 24 (12) (2009) 3498–3503.
[85] T. Ueki, D.J.F. Walker, P.-L. Tremblay, K.P. Nevin, J.E. Ward, T.L. Woodard, S. S. Nonnenmann, D.R. Lovley, Decorating the outer surface of microbially produced protein nanowires with peptides, ACS Synth. Biol. 8 (8) (2019) 1809–1817.
[86] X.i. Liu, S. Wang, A. Xu, L.i. Zhang, H. Liu, L.Z. Ma, Biological synthesis of high-conductive pili in aerobic bacterium *Pseudomonas aeruginosa*, Appl. Microbiol. Biotechnol. 103 (3) (2019) 1535–1544.
[87] K.P. Nevin, S.A. Hensley, A.E. Franks, Z.M. Summers, J. Ou, T.L. Woodard, O. L. Snoeyenbos-West, D.R. Lovley, Electrosynthesis of organic compounds from carbon dioxide is catalyzed by a diversity of acetogenic microorganisms, Appl. Environ. Microbiol. 77 (9) (2011) 2882–2886.
[88] K.P. Nevin, T.L. Woodard, A.E. Franks, Z.M. Summers, D.R. Lovley, R.R. Colwell, Microbial electrosynthesis: feeding microbes electricity to convert carbon dioxide and water to multicarbon extracellular organic compounds, ASM Microbe 1 (2) (2010).
[89] P. Aelterman, K. Rabaey, H.T. Pham, N. Boon, W. Verstraete, Continuous electricity generation at high voltages and currents using stacked microbial fuel cells, Environ Science and Technology 40 (10) (2006) 3388–3394.
[90] S.E. Oh, B.E. Logan, Voltage reversal during microbial fuel cell stack operation, J. Power Sources 167 (1) (2007) 11–17.